# Atomic-Scale Investigation of Defects, Dopants, and Lithium Transport in the $LiFePO_4$ Olivine-Type Battery Material

M. Saiful Islam,* Daniel J. Driscoll, Craig A. J. Fisher, and Peter R. Slater

*Materials Chemistry Group, Chemistry Division, SBMS, University of Surrey, Guildford GU2 7XH, United Kingdom*

*Received May 12, 2005. Revised Manuscript Received July 15, 2005*

Key issues relating to intrinsic defects, dopant incorporation, and lithium ion migration in the $LiFePO_4$ electrode material have been investigated using well-established atomistic modeling techniques. Our simulation model shows good reproduction of the observed olivine-type structure of $LiFePO_4$. The most favorable intrinsic defect is the Li−Fe "anti-site" pair in which a Li ion (on the M1 site) and an Fe ion (on the M2 site) are interchanged. This type of anti-site defect or "intersite exchange" has been observed in olivine silicates. The lowest Li migration energy is found for the pathway along the [010] channel, with a nonlinear, curved trajectory between adjacent Li sites. Trends in dopant substitution energetics of a range of cations with charges varying from +2 to +5 are also examined. Low favorable energies are found only for divalent dopants on the Fe site (such as Mn), which is in accord with experimental work. Our results suggest that, on energetic grounds, $LiFePO_4$ is not tolerant to aliovalent doping (e.g., Al, Ga, Zr, Ti, Nb, Ta) on either Li (M1) or Fe (M2) sites.

## 1. Introduction

The search for alternative cathode materials to replace the layered $LiCoO_2$ system conventionally used within rechargeable lithium batteries has generated considerable research activity.[1,2] The Co-based materials pose problems associated with cost and environmental hazard, particularly for large-scale applications (such as hybrid electric vehicles and back-up power systems). In this context, the olivine phosphates $LiMPO_4$ (e.g., M = Fe, Mn, Ni) have become a promising family of cathode materials exhibiting favorable electrochemical properties.[3−5]

The olivine structure is built up of $PO_4^{3-}$ tetrahedra, with the divalent M ions occupying corner-shared octahedral positions, and the Li ions located in chains of edge-sharing octahedra. Within this class of olivine phosphate, significant renewed activity[6−25] has focused on the Fe-based member, $LiFePO_4$. This is largely due to the high operating voltage (about 3.5 V vs $Li^+/Li$) for the $Fe^{3+}/Fe^{2+}$ couple, the large theoretical capacity to store charge per unit mass (ca. 170 mA h $g^{-1}$) and the good stability of the phosphate when in contact with common organic electrolytes. Such Fe-based oxides are also relatively low in cost and environmentally benign.

One of the key drawbacks with using $LiFePO_4$, however, is its low intrinsic electronic conductivity. Various synthesis and processing approaches have been employed to overcome this problem, which include using $LiFePO_4$/carbon conductive composites,[14,17,20] addition of dispersed metal powders,[18]

* Corresponding author: Dr. M. S. Islam. Tel.: +44 (0)1483 686844. Fax: +44 (0)1483 686851. E-mail: m.islam@surrey.ac.uk.

(1) Tarascon, J.-M.; Delacourt, C.; Prakash, R.; Morcrette, M.; Hedge, M.; Wurm, C.; Masquelier, C. *Dalton Trans.* **2004**, 2988.
(2) (a) Bruce, P. B. *Chem. Commun.* **1997**, 1817. (b) Whittingham, M. S. *Chem. Rev.* **2004**, *104*, 4271.
(3) Padhi, A. K.; Nanjundaswamy, K. S.; Goodenough, J. B. *J. Electrochem. Soc.* **1997**, *144*, 1188.
(4) Padhi, A. K.; Nanjundaswamy, K. S.; Masquelier, C.; Goodenough, J. B. *J. Electrochem. Soc.* **1997**, *144*, 2581.
(5) Masquelier, C.; Padhi, A. K.; Nanjundawsamy, K. S.; Goodenough, J. B. *J. Solid State Chem.* **1998**, *135*, 228.
(6) Chung, S.-Y.; Bloking, J. T.; Chiang, Y.-M. *Nat. Mater.* **2002**, *1*, 123.
(7) Ravet, N.; Abouimrane, A.; Armand, M. *Nat. Mater.* **2003**, *2*, 702.
(8) Herle, P. S.; Ellis, B.; Coombs, N.; Nazar, L. F. *Nat. Mater.* **2004**, *3*, 147.
(9) Delacourt, C.; Poizot, P.; Tarascon, J.-M.; Masquelier, C. *Nat. Mater.* **2005**, *4*, 254.
(10) (a) Deb, A.; Bergmann, U.; Cairns, E. J.; Cramer, S. P. *J. Phys. Chem. B* **2004**, *108*, 7046. (b) Prince, A. A. M.; Mylswamy, S.; Chan, T. S.; Liu, R. S.; Hannoyer, B.; Jean, M.; Shen, C. H.; Huang S. M.; Lee, J. F.; Wang, G. X. *Solid State Commun.* **2004**, *132*, 455.
(11) Morgan, D.; Van der Ven, A.; Ceder, G. *Electrochem. Solid-State Lett.* **2004**, *7*, A30.
(12) (a) Osorio-Guillen, J. M.; Holm, B.; Ahuja, R.; Johansson, B. *Solid State Ionics* **2004**, *167*, 221. (b) Burba, C. M.; Frech, R. *J. Electrochem. Soc.* **2004**, *151*, A1032.
(13) Ouyang, C. Y.; Shi, S. Q.; Wang, Z. X.; Li, H.; Huang, X. J.; Chen, L. Q. *J. Phys.: Condens. Matter* **2004**, *16*, 2265.
(14) Hsu, K. F.; Tsay, S. Y.; Hwang, B. J. *J. Mater. Chem.* **2004**, *14*, 2690.
(15) Chung, S.-Y.; Chiang, Y.-M. *Electrochem. Solid-State Lett.* **2003**, *6*, A278.
(16) Barker, J.; Saidi, M. Y.; Swoyer, J. L. *Electrochem. Solid-State Lett.* **2003**, *6*, A53.
(17) Doeff, M. M.; Hu, Y.; McLarnon, F.; Kostecki, R. *Electrochem. Solid-State Lett.* **2003**, *6*, A207.
(18) Croce, F.; D'Epifanio, A.; Hassoun, J.; Deptula, A.; Olczac, T.; Scrosati, B. *Electrochem. Solid-State Lett.* **2002**, *5*, A47.
(19) Prosini, P. P.; Lisi, M.; Zane, D.; Pasquali, M. *Solid State Ionics* **2002**, *148*, 45.
(20) Huang, H.; Yin, S.-C.; Nazar, L. F. *Electrochem. Solid-State Lett.* **2001**, *4*, A170.
(21) (a) García-Moreno, O.; Alvarez-Vega, M.; García-Alvarado, F.; García-Jaca, J.; Gallardo-Amores, J. M.; Sanjuán, M. L.; Amador, U. *Chem. Mater.* **2001**, *13*, 1570. (b) Goñi, A.; Lezama, L.; Pujana, A.; Arriortua, M. I.; Rojo, T. *J. Mater. Chem.* **2000**, *10*, 423.
(22) Yamada, A.; Chung, S. C.; Hinokuma, K. *J. Electrochem. Soc.* **2001**, *148*, A224.
(23) Andersson, A. S.; Kalsha, B.; Häggström, L.; Thomas, J. O. *Solid State Ionics* **2000**, *130*, 41.
(24) Yang, S.; Song, Y.; Zavalij, P. Y.; Whittingham, M. S. *Electrochem. Commun.* **2002**, *4*, 239.
(25) Delacourt, C.; Laffont, L.; Bouchet, R.; Wurm, C.; Leriche, J.-B.; Morcrette, M.; Tarascon, J.-M.; Masquelier, C. *J. Electrochem. Soc.*, **2005**, *152*, A913.

10.1021/cm050999v CCC: $30.25 © 2005 American Chemical Society
Published on Web 09/08/2005

and doping with "supervalent" cations.[6] In particular, Chung et al.[6] reported that low-level doping of $LiFePO_4$ by a range of aliovalent ions (e.g., $Mg^{2+}$, $Al^{3+}$, $Ti^{4+}$, $Zr^{4+}$, $Nb^{5+}$) increases the electronic conductivity by a factor of more than $10^8$ (reaching values of greater than $10^{-2}$ S cm$^{-1}$ at room temperature); they argued that doping of cation-deficient phases is charge-compensated by $Fe^{3+}$, thereby introducing p-type conductivity, although they also acknowledged that the precise site occupancy ($Li^+$ vs $Fe^{2+}$) of specific dopants has yet to be established.

Not surprisingly these doping results have stimulated considerable interest and controversy in the lithium battery field. There is much debate concerning the precise defect chemistry and whether the observed increase in electronic conductivity is a true lattice doping effect or is due to other effects such as carbon contamination from carbon-containing precursors[7] and/or the formation of highly conducting metal phosphides from $LiFePO_4$ reduction.[7,8] Enhanced conductivity in doped (and undoped) $LiMPO_4$ (M = Fe, Ni) has also been found via a non-carbon "nano-network" of metal-rich phosphides.[8]

In terms of defect chemistry, studies of related $Li_{1-3x}Fe_xNiPO_4$ phases suggest that cation vacancies can be accommodated in the olivine structure,[24] while density functional theory (DFT)-based calculations[11,13] on $LiMPO_4$ (M = Fe, Mn, Co, Ni) have found low activation barriers for Li ion motion through one-dimensional channels. More recently, experimental evidence for the existence of a solid-solution $Li_xFePO_4$ ($0 < x < 1$) at 450 °C and two room-temperature metastable phases (with $x = 0.75$ and 0.5) has been reported.[9]

It is clear that the underlying defect and transport properties of oxide cathode materials are complex on the atomic scale but are crucial to the greater understanding of their structure−property relationships and electrochemical behavior. The present study uses well-established atomistic simulation techniques to investigate key issues related to point defects, dopants, and lithium ion migration in the $LiFePO_4$ material, with reference to experimental results where possible. Such techniques are based upon effective energy minimization procedures, which are well-suited to treating the extensive lattice relaxation (up to several hundred ions) around charged defects, dopant species, and migrating ions in polar inorganic solids.[26,27]

This work extends our analogous computational studies of other lithium battery materials including $LiMn_2O_4$ spinel[28] and layered $LiNi_{0.5}Mn_{0.5}O_2$.[29] In this study we have focused on the $LiFePO_4$ phase and carried out a detailed examination of the relative energetics of the formation of intrinsic defects, the incorporation of dopants and corresponding charge-compensation mechanisms, and the possible pathways for lithium ion migration.

## 2. Simulation Methods and Structural Modeling

**2.1. Methods.** This study employs well-established atomistic modeling techniques, which are reviewed in detail elsewhere,[26,27] and, hence, only a brief description will be given here. The interactions between ions in the crystalline solid are represented in terms of a long-range Coulombic term plus an analytical function representing short-range repulsive and van der Waals interactions. These short-range interactions were modeled using the Buckingham potential:

$$V_{ij}(r_{ij}) = A \exp(-r_{ij}/\rho) - C/r_{ij}^{\,6} \qquad (1)$$

where $r$ is the interatomic separation and $A$, $\rho$, and $C$ are ion−ion potential parameters. An additional three-body term was also used in this work, which has been widely employed in the modeling of silicates,[26] aluminosilicates (zeolites),[26,30] and more recently, apatite materials.[31,32] This is necessary to take account of the angle-dependent nature of the $SiO_4$ or $PO_4$ tetrahedral units. Here it is defined for each O−P−O bond and takes the form of a harmonic angle-bending potential about the central P ion:

$$V_{3\text{-body}} = {}^1/_2 k(\theta - \theta_0)^2 \qquad (2)$$

where $k$ is the force constant and $\theta_0$ is the equilibrium bond angle. It should be stressed (as argued previously)[26] that employing such a formal charge model does not necessarily mean that the electron distribution corresponds to a fully ionic system and that the validity of the potential model is assessed primarily by its ability to reproduce observed crystal properties. In practice, it is found that such models work well, even for compounds such as aluminophosphates,[33] gallium phosphates,[34] and olivine silicates,[35] in which there is a significant degree of covalency. For example, recent studies of Henson et al.[33] have used such potentials to reproduce a whole series of experimental structures and stability trends of aluminophosphates. Another key benefit of the formal charge model is that there are no ambiguities about the charge state when considering isovalent or aliovalent dopant substitution.

Because charged defects will polarize other ions in the lattice, electronic polarization must be incorporated into the potential model. The shell model[26,27] provides a simple description of such effects (particularly for the polarizable oxygen) and has proven to be effective in simulating the dielectric properties of ceramic oxides. Efficient energy minimization of the crystal lattice is carried out using Newton−Raphson (second derivative) methods using symmetry in the optimization procedures.

(26) Catlow, C. R. A., Ed. *Computer Modelling in Inorganic Crystallography*; Academic Press: San Diego, 1997.
(27) Hill, J. R.; Freeman, C. M.; Subramanian, L. In *Reviews in Computational Chemistry*; Liphowitz, K. B., Boyd, D. B., Eds.; Wiley: New York, 2000; Vol. 16.
(28) (a) Ammundsen, B.; Roziere, J.; Islam, M. S. *J. Phys. Chem. B* **1997**, *101*, 8156. (b) Ammundsen, B.; Burns, G. R.; Islam, M. S.; Kanoh, H.; Rozière, J. *J. Phys. Chem. B* **1999**, *103*, 5175.
(29) Islam, M. S.; Davies, R. A.; Gale, J. D. *Chem. Mater.* **2003**, *15*, 4280.
(30) (a) Higgins, F. M.; de Leeuw, N. H.; Parker, S. C. *J. Mater. Chem.* **2002**, *12*, 124. (b) Channon, Y. M.; Catlow, C. R. A.; Gorman, A. M.; Jackson, R. A. *J. Phys. Chem. B* **1998**, *102*, 4045.
(31) (a) Islam, M. S.; Tolchard, J. R.; Slater, P. R. *Chem. Commun.* **2003**, 1486. (b) Tolchard, J. R.; Slater, P. R.; Islam, M. S. *J. Mater. Chem.* **2003**, *13*, 1956.
(32) de Leeuw, N. H.; Mkhonto, D. *Chem. Mater.* **2003**, *15*, 1567.
(33) Henson, N. J.; Cheetham, A.; Gale, J. D. *Chem. Mater.* **1996**, *8*, 664.
(34) Girard, S.; Gale, J. D.; Mellot-Draznieks, C.; Ferey, G. *Chem. Mater.* **2001**, *13*, 1732.
(35) Walker, A. M.; Wright, K.; Slater, B. *Phys. Chem. Miner.* **2003**, *30*, 536.

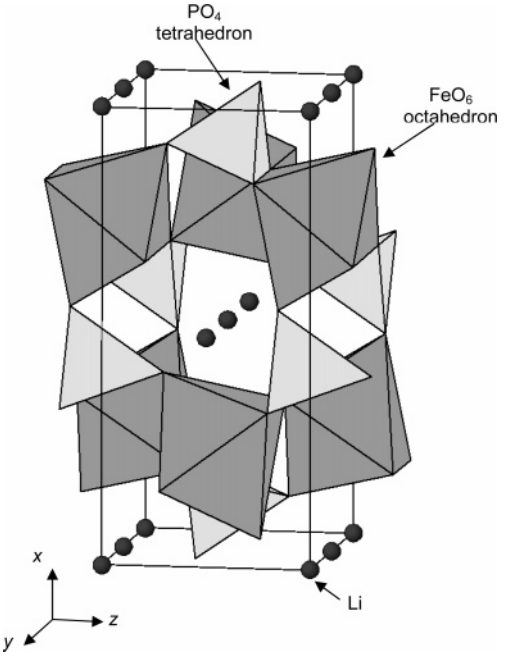


**Figure 1.** Structure of $LiFePO_4$.

An important feature of the defect calculations is the treatment of lattice relaxation about the charged defect, dopant species, or migrating ion. The Mott−Littleton approach[26] (embodied in the GULP code)[36] is to partition the crystal lattice into two regions so that ions in a spherical inner region (of more than 1000 ions) surrounding the defect are relaxed explicitly. In contrast, the remainder of the crystal (typically >3000 ions), where the defect forces are relatively weak, is treated by more approximate quasi-continuum methods. In this way, long-range lattice relaxation is modeled effectively and the crystal is not considered simply as a rigid lattice. It is worth noting that explicit relaxation of such a large number of lattice ions around defect species is not easily treated by DFT-based computational methods. The latter, of course, can be used to provide valuable information on electronic structure and redox potentials.

**2.2. Structural Modeling of $LiFePO_4$.** The starting point for the computational study was the simulation of the crystal structure. The olivine structure of $LiFePO_4$ is orthorhombic (space group *Pnma*)[23,37] with a slightly distorted hexagonal close-packed oxygen array. The P atoms occupy tetrahedral sites, while the Li ions are located in chains of edge-sharing octahedra (denoted as M1 sites) and the divalent Fe ions occupy corner-sharing octahedra (M2 sites), as shown in Figure 1. Recent X-ray absorption near-edge structure (XANES) and Mossbauer studies[10] of $LiFePO_4$ confirm that iron is present in the 2+ state.

As there is limited previous work relating to the atomistic modeling of olivine phosphate materials, our initial approach to simulating the $LiFePO_4$ structure was to use a selection of published interatomic potentials. The potentials for the Li−O and Fe−O interactions were transferred from analogous lithium insertion studies of $LiMn_2O_4$[28] and $Fe_3O_4$.[38]

**Table 1. Short-Range Potential Parameters for $LiFePO_4$**

(a) Two-Body

| interaction | $A$ (eV) | $\rho$ (Å) | $C$ (eV·Å$^6$) | $Y$ (e) | $K$ (eV·Å$^{-2}$) |
|---|---|---|---|---|---|
| $Li^+-O^{2-}$ | 632.1018 | 0.2906 | 0.0 | 1.0 | 99 999.0 |
| $Fe^{2+}-O^{2-}$ | 1105.2409 | 0.3106 | 0.0 | 2.997 | 19.26 |
| $P^{5+}-O^{2-}$ | 897.2648 | 0.3577 | 0.0 | 5.0 | 99 999.0 |
| $O^{2-}-O^{2-}$ | 22 764.3 | 0.149 | 44.53 | −2.96 | 65.0 |

(b) Three-Body

| bonds | $k$ (eV·rad$^{-2}$) | $\theta_0$ (deg) |
|---|---|---|
| $O^{2-}-P^{5+}-O^{2-}$ | 1.322626 | 109.47 |

**Table 2. Calculated and Experimental[37] Structural Parameters of $LiFePO_4$ (Space Group *Pnma*)**

(a) Unit Cell Parameters

| parameter | calcd (Å) | exptl (Å) | Δ (Å) |
|---|---|---|---|
| *a* | 10.3713 | 10.3377 | 0.0336 |
| *b* | 6.0216 | 6.0112 | 0.0104 |
| *c* | 4.6695 | 4.6950 | −0.0255 |

(b) Bond Lengths

| ion pair | calcd (Å) | exptl (Å) | Δ (Å) |
|---|---|---|---|
| P−O(1) | 1.510 | 1.525 | −0.015 |
| P−O(2) | 1.557 | 1.539 | 0.018 |
| P−O(3) (×2) | 1.571 | 1.558 | 0.013 |
| Li−O(1) (×2) | 2.189 | 2.174 | 0.015 |
| Li−O(2) (×2) | 2.103 | 2.086 | 0.017 |
| Li−O(3) (×2) | 2.235 | 2.194 | 0.041 |
| Fe−O(1) | 2.190 | 2.199 | −0.009 |
| Fe−O(2) | 2.050 | 2.115 | −0.065 |
| Fe−O(3) (×2) | 2.057 | 2.061 | −0.004 |
| Fe−O(3) (×2) | 2.239 | 2.253 | −0.014 |

(c) Bond Angles

| ion trimer | calcd (deg) | exptl (deg) | Δ (deg) |
|---|---|---|---|
| O(3)−P−O(3) | 101.059 | 103.585 | −2.5 |
| O(2)−P−O(3) (×2) | 105.220 | 106.466 | −1.2 |
| O(1)−P−O(2) | 114.204 | 113.184 | 1.0 |
| O(1)−P−O(3) (×2) | 114.615 | 113.189 | 1.4 |

(d) Dielectric Constants

| | calcd |
|---|---|
| static, $\epsilon_0$ | 11.58 |
| high frequency, $\epsilon_{inf}$ | 4.74 |

We found that the best structural reproduction was achieved using the O−P−O three-body terms from recent studies on apatite phosphates[32] with slight refinement of the P−O and O−O pair potentials transferred from simulations of aluminophosphates.[33]

The final refined interatomic potentials used in the present study are listed in Table 1. The structure of $LiFePO_4$ was first optimized (energy minimized) under constant pressure conditions, which allows both lattice parameters (cell volume) and ion positions to relax. The calculated structural parameters are listed with experimental data in Table 2 and show good agreement. It can be seen that our calculated unit cell parameters deviate by less than 0.04 Å from experimental values, and all bond lengths and bond angles are reproduced to within 0.06 Å and 2.5°, respectively. The calculated dielectric constants are also listed, indicating relatively low values. Despite the lack of any corresponding experimental data for $LiFePO_4$, our calculated dielectric constants are consistent with measured values for other inorganic phosphates [such as $AlPO_4$, $NaBePO_4$, and $LiAlPO_4(OH)$], which fall in the

(36) Gale, J. D. *J. Chem. Soc., Faraday Trans.* **1997**, *93*, 629.
(37) Rousse, G.; Rodriguez-Carvajal, J.; Patoux, S.; Masquelier, C. *Chem. Mater.* **2003**, *15*, 4082.
(38) Islam, M. S.; Catlow, C. R. A. *J. Solid State Chem.* **1988**, *77*, 180.

range 4.6−10.7 (as listed in the detailed compilation by Shannon).[39]

In general, the simulations show good reproduction of the observed complex structure of $LiFePO_4$, thus supporting the validity of the potentials used for the subsequent defect calculations. We have focused on defect, dopant, and Li migration properties; the topic of $Li_xFePO_4$ ($x < 1.0$) phase stability merits future investigation. To our knowledge, these studies are the first detailed survey of the defect chemistry of $LiFePO_4$ employing atomistic simulation methods.

## 3. Results and Discussion

**3.1. Intrinsic Atomic Defects.** A series of calculations were carried out in which the energies of isolated point defects (vacancies and interstitials) in $LiFePO_4$ were first obtained. As noted, lattice relaxation associated with charged defects is treated effectively by our simulation approach, in which there is explicit energy minimization within a spherical inner region of more than 1000 ions. This is important for charged defects that can have a long-range electrostatic effect within the crystalline lattice.

Combining the energies of these point defects, we then derived energies of formation for Frenkel and Schottky-type disorder. For example, in Kroger−Vink notation, these take the general form

Li Frenkel:

$$Li_{Li}^{\times} \rightarrow V'_{Li} + Li_i^{\bullet} \quad (3)$$

Fe Frenkel:

$$Fe_{Fe}^{\times} \rightarrow V''_{Fe} + Fe_i^{\bullet\bullet} \quad (4)$$

O Frenkel:

$$O_O^{\times} \rightarrow V_O^{\bullet\bullet} + O_i'' \quad (5)$$

Schottky:

$$Li_{Li}^{\times} + Fe_{Fe}^{\times} + P_P^{\times} + 4O_O^{\times} \rightarrow V'_{Li} + V''_{Fe} + V''''_P + 4V_O^{\bullet\bullet} + LiFePO_4 \quad (6)$$

$Li_2O$ Schottky-like:

$$2Li_{Li}^{\times} + O_O^{\times} \rightarrow 2V'_{Li} + V_O^{\bullet\bullet} + Li_2O \quad (7)$$

FeO Schottky-like:

$$Fe_{Fe}^{\times} + O_O^{\times} \rightarrow V''_{Fe} + V_O^{\bullet\bullet} + FeO \quad (8)$$

We also examined the Li−Fe "anti-site" pair defect involving one $Li^+$ (radius = 0.74 Å) and one $Fe^{2+}$ (radius = 0.78 Å) interchanged between their two nonequivalent M1 and M2 octahedral sites; this can be described by the following equation:

$$Fe_{Fe}^{\times} + Li_{Li}^{\times} \rightarrow Li'_{Fe} + Fe_{Li}^{\bullet} \quad (9)$$

This type of defect is worth considering because "intersite cation exchange" effects have been observed in olivine silicates such as $MgFeSiO_4$,[40−42] and anti-site behavior is found in the layered battery materials such as $LiNiO_2$, in which some Li is found on the transition metal sites.[2]

**Table 3. Energies of Intrinsic Atomic Defects in $LiFePO_4$**

| defect | eq | energy (eV) |
|---|---|---|
| Li Frenkel | 3 | 2.15 |
| Fe Frenkel | 4 | 5.58 |
| O Frenkel | 5 | 5.46 |
| full Schottky | 6 | 25.30 |
| $Li_2O$ Schottky-like | 7 | 6.33 |
| FeO Schottky-like | 8 | 5.58 |
| Li/Fe anti-site pair (isolated) | 9 | 1.13 |
| Li/Fe anti-site pair (cluster) | 9 | 0.74 |

The calculated energies for all these types of intrinsic defects are listed in Table 3, from which three main points can be made. First, the high energies associated with the formation of Fe Frenkel, O Frenkel, and Schottky defects suggest that such intrinsic defects are not significant in this material. In particular, the results support models in which simple oxide ion vacancies and interstitials are unlikely to be important in olivine-type phosphates.

Second, the most significant result is that the lowest energy is found for the Li−Fe anti-site pair defect (eq 9) in which a Li ion (on the M1 site) and an Fe ion (on the M2 site) are interchanged. Our analysis of the local relaxation around the $Li'_{Fe}$ and $Fe_{Li}^{\bullet}$ defects indicates very small changes of less than 0.08 Å in the local M−O octahedral bond lengths. This result suggests the possibility of a small degree of anti-site disorder of Li and Fe ions over M1 and M2 octahedral sites. Indeed, in the mineralogy field this type of anti-site defect or "intersite exchange" has been discussed in relation to olivine silicates such as $MgFeSiO_4$ and $MnFeSiO_4$; in situ neutron diffraction studies have found substantial temperature-dependent partitioning of the two divalent ions (e.g., Mg−Fe) between the structurally distinct octahedral sites.[40−42]

The measurements on olivine silicates of Henderson et al.[40] also give Mg−Fe intersite "exchange energies" of about 0.1−0.2 eV. In comparison, our higher Li−Fe anti-site energies (ca. 0.7 eV) for $LiFePO_4$ suggest that the degree of anti-site disorder is much lower (ca. 1−2 mol %) at ambient temperatures. It is interesting to note that Yang et al.[24] reported that Rietveld analysis of hydrothermally formed $LiFePO_4$ suggests 3−5% occupation of Li sites by Fe. As discussed previously,[11,24] these anti-site defects, particularly Fe on Li sites, could have an effect on Li ion conduction, a point we return to in the next section.

It is well-known that Coulombic and elastic interactions between defects can lead to association or clustering. We have, therefore, considered the binding (association) energy of nearest-neighbor $Li'_{Fe}$ and $Fe_{Li}^{\bullet}$ anti-site defects in the form of a ($Li'_{Fe}$, $Fe_{Li}^{\bullet}$) pair cluster. The calculated binding energy is −0.4 eV with respect to the isolated defects, which reduces the energy for formation of an anti-site pair defect to 0.74 eV (Table 3).

(39) Shannon, R. D. *J. Appl. Phys.* **1993**, *73*, 348.
(40) Henderson, C. M. B.; Knight, K. S.; Redfern, S. A. T.; Wood, B. J. *Science* **1996**, *271*, 1713.
(41) (a) Artioli, G.; Rinaldi, R.; Wilson, C. C.; Zanazzi, P. F. *Am. Mineral.* **1995**, *80*, 197. (b) Redfern, S. A. T.; Artioli, G.; Rinaldi, R.; Henderson, C. M. B.; Knight, K. S.; Wood, B. J. *Phys. Chem. Miner.* **2000**, *27*, 630.
(42) Henderson, C. M. B.; Redfern, S. A. T.; Smith, R. I.; Knight, K. S.; Charnock, J. M. *Am. Mineral.* **2001**, *86*, 1170.

These defect clusters may be too small to be detected by neutron powder diffraction. In this context, it is worth noting that X-ray absorption studies of $(Mg,Ni)_2SiO_4$ olivines indicate Ni clustering as well as Ni-rich and Mg-rich nanodomains.[42] In any case, our results clearly suggest the need for further structural work (e.g., neutron diffraction, Li NMR) to examine possible Li−Fe anti-site defects and defect clustering in $LiFePO_4$. We recognize, of course, that diffraction analysis of local features comprised of small Li ions will not be straightforward.

Finally, Table 3 reveals a relatively low energy for the Li Frenkel defect (eq 3). This suggests that a minor concentration of such vacancy and interstitial defects could be present, which may contribute to any intrinsic ionic conductivity. From a detailed search of the potential energy surface, the unit cell of $LiFePO_4$ is found to contain eight symmetry-equivalent $Li^+$ interstitial positions (on either side of each lattice Li site), for example, the interstitial positions (0.38, 0.45, 0.42) and (0.62, 0.55, 0.58) about the (0.5, 0.5, 0.5) Li site in fractional coordinates (in units of a, b, and c). The calculations find that such a Li interstitial defect causes considerable local relaxation in which the adjacent lattice Li ion is displaced by about 1.3 Å into its second neighboring interstitial position, leading to a separation between the two Li ions of 2.6 Å. Interestingly, the Li interstitial ion is coordinated to four neighboring O ions in a distorted tetrahedral environment with short Li−O separations of 1.85−2.06 Å (compared to the average Li−O bond length of 2.2 Å). This suggests strong local interactions and possible trapping of the interstitial ion, which would inhibit defect mobility.

Such Li interstitial defects would be difficult to probe by X-ray diffraction alone. In this context, it is worth noting that there has been conflicting debate about whether a minor concentration of lithium is located at "midway" sites in phosphate structures related to the Na superionic conductor (NASICON) [e.g., $LiZr_2(PO_4)_3$].[43]

**3.2. Li Ion Migration.** Examination of the intrinsic Li ion mobility in $LiFePO_4$ is of vital interest when considering its use as a cathode material in lithium batteries. Simulation methods can greatly enhance our understanding of the defect process or migration pathway by evaluating the activation energies for various possible mechanisms at the atomic level. It is worth recalling that our simulation approach treats long-range relaxation and polarizability about the migrating Li ion because the structure is not considered simply as a hard-sphere lattice with fixed ions.

Three main migration mechanisms were considered within the olivine structure (space group *Pnma*) involving conventional vacancy hopping between neighboring Li positions (illustrated in Figure 2) as discussed previously.[11] These were mechanism A, migration between adjacent M1 sites along the [010] direction (parallel to the *y* axis); mechanism B, migration between the *y*-axis channels along the [001] direction (parallel to the *z* axis); and mechanism C, migration also across channels but in the [101] direction.

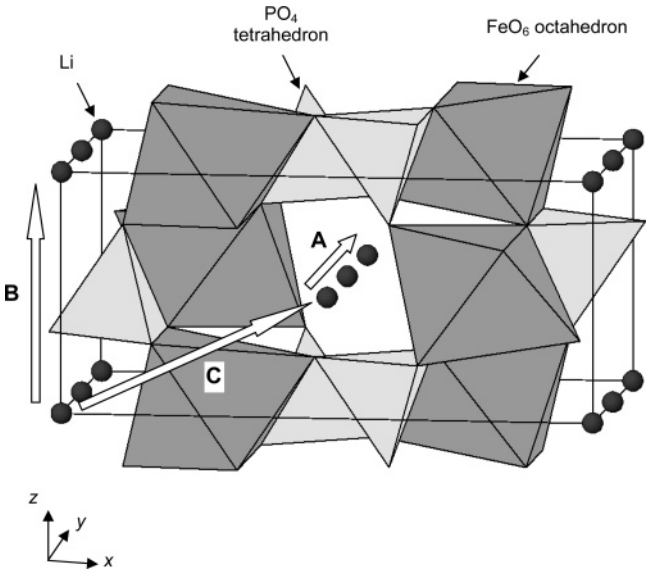


**Figure 2.** Li ion migration paths in a unit cell of $LiFePO_4$. Mechanism A, [010] direction; mechanism B, [001] direction; mechanism C, [101] direction.

**Table 4. Mechanisms and Energies of Li Ion Migration in $LiFePO_4$**

| mechanism[a] | path | Li−Li separation (Å) | $E_{mig}$ (eV) |
|---|---|---|---|
| A: $Li_{Li}^{\times} \rightarrow V'_{Li}$ | [010] | 3.01 | 0.55 |
| B: $Li_{Li}^{\times} \rightarrow V'_{Li}$ | [001] | 4.67 | 2.89 |
| C: $Li_{Li}^{\times} \rightarrow V'_{Li}$ | [101] | 5.69 | 3.36 |

[a] Illustrated in Figure 2.

Energy profiles for these mechanisms can be mapped out by calculating the energy of the migrating Li ion along the diffusion path. In this way the position of highest potential energy (i.e., the "saddle point" configuration) can be identified from which the migration energy is derived; this is an approach used successfully in numerous previous studies on oxide ion and cation migration in complex oxides.[26,31,44,45] We note that our simulations relate to the very low concentration regime (dilute limit) with no interactions between migrating Li ions. The resulting migration energies for the three mechanisms considered are reported in Table 4.

Examination of the results reveals a low-energy pathway (0.55 eV) for Li vacancy migration along the Li ion channel in the [010] direction (mechanism A in Figure 2). High-energy barriers of more than 2.8 eV are calculated for the other two mechanisms. These results indicate high Li ion mobility down the [010] channel. This is consistent with recent DFT-based simulations of Morgan et al.,[11] although they find a much lower energy barrier of 0.27 eV, from which a diffusion constant, *D*, of $10^{-8}$ $cm^2$ $s^{-1}$ is estimated.

It is often assumed that the migrating ion takes the shortest path between adjacent sites, that is, a direct linear jump. However, detailed analysis of our simulations for the favored migration mechanism (A) along the [010] channel reveals a small deviation from the linear (straight) route involving a curved path between adjacent Li sites. The magnitude of this deviation at the saddle point is about 0.5 Å away from the

(43) (a) Catti, M.; Comotti, A.; Di Blas, S. *Chem. Mater.* **2003**, *15*, 1628. (b) Aatiq, A.; Menetrier, M.; Croguennec, L.; Suard, E.; Delmas, C. *J. Mater. Chem.* **2002**, *12*, 2971.

(44) (a) Islam, M. S. *J. Mater. Chem.* **2000**, *10*, 1027. (b) Khan, M. S.; Islam, M. S.; Bates, D. R. *J. Phys. Chem. B* **1998**, *102*, 3099.

(45) Pirzada, M.; Grimes, R. W.; Minervini, L.; Maguire, J. F.; Sickafus, K. E. *Solid State Ionics* **2001**, *140*, 201.

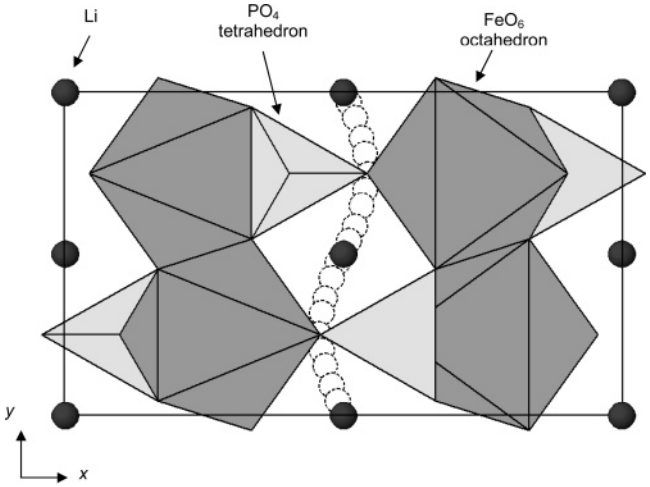


**Figure 3.** Curved trajectories for Li ion migration between sites in the [010] direction (mechanism A). The diffusion path lies out of the $x-y$ plane.

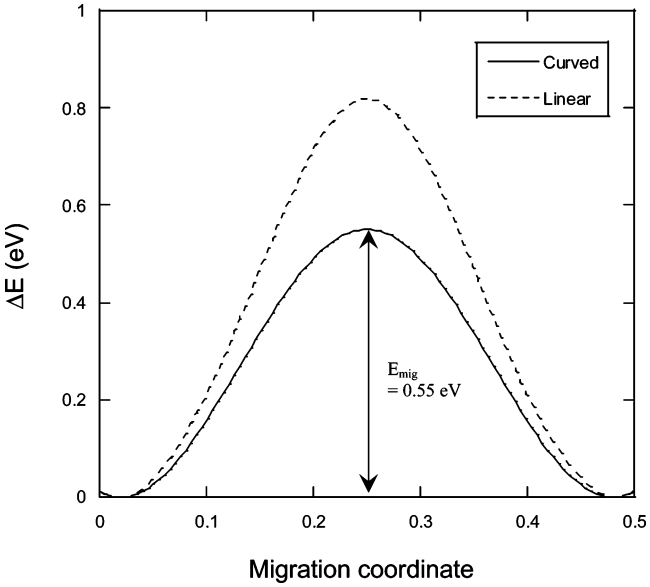


**Figure 4.** Energy profile of Li migration via mechanism A ([010] direction) for linear and curved paths between adjacent Li sites.

**Table 5. Displacement of Neighboring Ions Away from the Migrating Li Ion at the Saddle Point for Mechanism A**

| ion | Δ (Å) | ion | Δ (Å) | ion | Δ (Å) |
|---|---|---|---|---|---|
| Fe | 0.18 | P | 0.08 | O(1) | 0.20 |
| Fe | 0.05 | P | 0.12 | O(2) | 0.18 |

linear path (and away from the adjacent P ion). This produces a "wavelike" trajectory for long-range migration as illustrated in Figure 3 and results in a lower migration energy than if the Li ion followed a direct, linear path; the energy profiles for linear versus curved paths are shown in Figure 4.

At the saddle point configuration for this pathway, significant local relaxation is calculated. We find displacements for the neighboring P, Fe, and O ions of up to 0.1−0.2 Å away from the migrating Li ion (listed in Table 5). Such relaxation assists Li ion mobility by modifying the size of the opening at the saddle point "bottleneck". These results again emphasize the importance of including lattice relaxation effects when investigating possible migration paths; such effects would be missing in, for example, a purely empirical ion size approach.

It is worth noting that analogous nonlinear, curved paths have been found from atomistic simulation[44] and neutron diffraction[46] studies of oxide ion migration in the $LaGaO_3$ perovskite. In addition, recent studies of lithium manganese spinel materials using synchrotron X-ray diffraction, electron density distribution analysis, and extended X-ray absorption fine structure (EXAFS) techniques have found complicated Li hopping routes in conjuction with local lattice distortion.[47] Indeed, one of the aims of the present study is to stimulate similar experimental work on $LiFePO_4$ to probe actual Li migration pathways.

Although there are limited Li ion conductivity data for direct comparison, our calculated value of 0.55 eV is consistent with experimental activation energies of 0.54 and 0.63 eV for pure $LiFePO_4$ from direct current conductivity and impedance spectroscopy measurements, respectively.[25] However, we recognize that the precise carrier species (polaron versus ionic) and the formation term have not been clearly established and that some computational studies calculate much lower values (<0.3 eV).[11] Nevertheless, our calculated migration energy is also compatible with experimental activation energies for Li ion conductivity in other framework-structured or NASICON-type phosphate materials.[48]

Relatively low diffusion coefficients ($D_{Li}$) on the order of $1.8 \times 10^{-14}$ cm$^2$ s$^{-1}$ have been found for $LiFePO_4$ using galvanostatic intermittent titration techniques.[19] However, we should note that there are difficulties in measuring Li diffusion coefficients electrochemically in a two-phase regime (i.e., $LiFePO_4-FePO_4$) because the kinetics of migration of the phase boundary itself are incorporated within the diffusion data.

In summary, we predict highly anisotropic behavior with preferential Li ion migration along the one-dimensional [010] channels via a nonlinear, curved trajectory between Li sites. This mechanism is likely to be general for all $LiMPO_4$ olivine-type materials. With such a one-dimensional pathway there is also the possibility that long-range Li conduction will be easily blocked. For instance, because our defect calculations suggest that Li−Fe anti-site defects (eq 9) are intrinsic to $LiFePO_4$, it may be difficult to avoid Fe on Li sites blocking the diffusion pathways down [010] channels, unless the anti-site defect itself is highly mobile. This would obviously inhibit long-range Li migration and influence the electrochemical kinetics during Li extraction.

Finally, we note that preliminary calculations on Li interstitial migration indicate a possible indirect mechanism, although we recognize that the intrinsic concentration of such interstitial defects is unlikely to be high enough to affect the diffusion properties. Further work in this area is currently underway and includes molecular dynamics simulations to probe cooperative diffusion mechanisms.

**3.3. Dopant Substitution.** As noted, compositions with very low dopant levels such as $Li_{0.99}M_{0.01}FePO_4$ (where M = $Mg^{2+}$, $Al^{3+}$, $Zr^{4+}$, $Nb^{5+}$) have been reported,[6] although it

(46) Yashima, M.; Nomura, K.; Kageyama, H.; Miyazaki, Y.; Chitose, N.; Adachi, K. *Chem. Phys. Lett.* **2003**, *380*, 391.
(47) Ishizawa, N.; Du Boulay, D.; Hayatsu, M.; Kuze, S.; Matsushima, Y.; Ikuta, H.; Wakihara, M.; Tabira, Y.; Hester, J. R. *J. Solid State Chem.* **2003**, *174*, 167.
(48) Sebastion, L.; Gopalakrishnan, J. *J. Mater. Chem.* **2003**, *13*, 433.

is acknowledged that the precise site occupancy (Li versus Fe) of specific dopants has yet to be established. These results have stimulated considerable debate about the precise defect properties and whether the observed enhancement in electronic conductivity is due to solid-state cation doping or to other effects such as carbon contamination and/or phosphide formation.

Cation doping of the $LiFePO_4$ material raises key questions in relation to the favored substitution site (M1 versus M2), the type of compensating defect, and whether the doping process is favorable on energetic grounds. Our simulation methods can address these issues by generating quantitative estimates of the relative energies of different modes of dopant substitution. In this way, our results can provide a useful systematic guide to the site selectivity for different dopant species and to trends in dopant solubility. We have, therefore, examined a range of dopants including divalent (e.g., Mg, Mn, Co), trivalent (e.g., Al, Ga, Y), tetravalent (e.g., Zr, Ti), and pentavalent (e.g., Nb, Ta) ions, which constitute a wider survey than current experimental reports.

For aliovalent ("donor") dopants (such as $Mg^{2+}$ on $Li^+$ or $Al^{3+}$ on $Fe^{2+}$), the type of charge-compensating defect has not been clearly established from experiment and could be either Li vacancies, Fe vacancies, or electronic species ($Fe^+$). Our initial calculations find that the lowest energy compensation mechanism involves Fe vacancies. Dopant substitution of $M^{2+}$, $M^{3+}$, $M^{4+}$, and $M^{5+}$ ions (as MO, $M_2O_3$, $MO_2$, and $M_2O_5$ compounds, respectively) can then be represented by the following series of defect equations (normalized to one dopant substitutional, $M_{Li}$ or $M_{Fe}$):

$M^{2+}$ on Li:

$$MO + Li_{Li}^{\times} + \frac{1}{2}Fe_{Fe}^{\times} \rightarrow M_{Li}^{\bullet} + \frac{1}{2}V_{Fe}'' + \frac{1}{2}Li_2O + \frac{1}{2}FeO \quad (10)$$

$M^{2+}$ on Fe:

$$MO + Fe_{Fe}^{\times} \rightarrow M_{Fe}^{\times} + FeO \quad (11)$$

$M^{3+}$ on Li:

$$\frac{1}{2}M_2O_3 + Li_{Li}^{\times} + Fe_{Fe}^{\times} \rightarrow M_{Li}^{\bullet\bullet} + V_{Fe}'' + \frac{1}{2}Li_2O + FeO \quad (12)$$

$M^{3+}$ on Fe:

$$\frac{1}{2}M_2O_3 + \frac{3}{2}Fe_{Fe}^{\times} \rightarrow M_{Fe}^{\bullet} + \frac{1}{2}V_{Fe}'' + \frac{3}{2}FeO \quad (13)$$

$M^{4+}$ on Li:

$$MO_2 + Li_{Li}^{\times} + \frac{3}{2}Fe_{Fe}^{\times} \rightarrow M_{Li}^{\bullet\bullet\bullet} + \frac{3}{2}V_{Fe}'' + \frac{1}{2}Li_2O + \frac{3}{2}FeO \quad (14)$$

$M^{4+}$ on Fe:

$$MO_2 + 2Fe_{Fe}^{\times} \rightarrow M_{Fe}^{\bullet\bullet} + V_{Fe}'' + 2FeO \quad (15)$$

$M^{5+}$ on Li:

$$\frac{1}{2}M_2O_5 + Li_{Li}^{\times} + 2Fe_{Fe}^{\times} \rightarrow M_{Li}^{\bullet\bullet\bullet\bullet} + 2V_{Fe}'' + \frac{1}{2}Li_2O + 2FeO \quad (16)$$

$M^{5+}$ on Fe:

$$\frac{1}{2}M_2O_5 + \frac{5}{2}Fe_{Fe}^{\times} \rightarrow M_{Fe}^{\bullet\bullet\bullet} + \frac{3}{2}V_{Fe}'' + \frac{5}{2}FeO \quad (17)$$

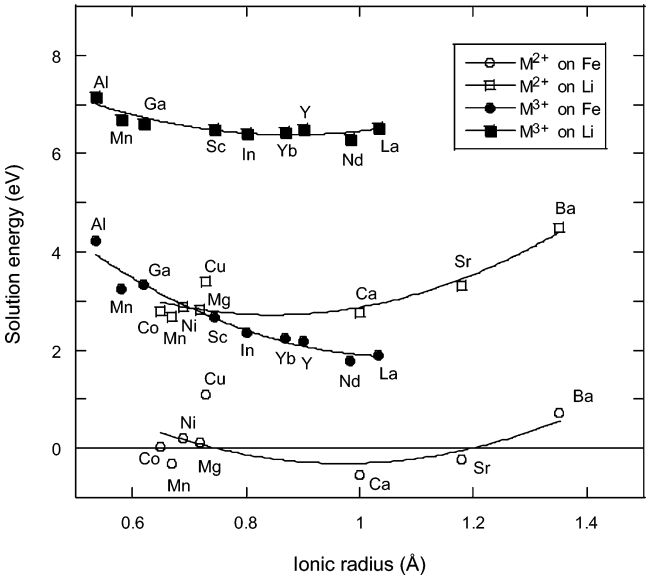


**Figure 5.** Solution energies of divalent (eqs 10 and 11) and trivalent (eqs 12 and 13) dopants on Li and Fe sites as a function of ion size. (Lines are a guide for the eye only.)

The energies of these dopant substitution or "solution" reactions can be evaluated by combining appropriate defect and lattice energy, $U_{lat}$, terms; for example, the solution energy, $E_{sol}$, for eq 11 is derived using the following:

$$E_{sol} = E(M_{Fe}^{\times}) + U_{lat}(FeO) - U_{lat}(MO) \quad (18)$$

These defect simulations are at the dilute limit in which an isolated dopant ion is inserted into the lattice. Although there are some uncertainties in the precise magnitude of the solution energies because of the large lattice energies involved, such a systematic approach has been applied successfully to a variety of other oxide materials.[49−51] The interatomic potentials for the dopant species[52] are exactly those of the corresponding binary oxides that have been derived to reproduce their crystal structures and have been used in previous studies of dopant incorporation.[49−51] The resulting solution energies for a wide range of $M^{2+}$, $M^{3+}$, $M^{4+}$, and $M^{5+}$ dopants are presented as a function of ion size in Figures 5 and 6.

Examination of the results reveals two main points. First, low favorable energies are found only for divalent dopants (e.g., Mg, Mn, Co, Ca) on the Fe site (Figure 5); the most unfavorable divalent dopants are Cu and Ba. This isovalent substitution process does not require charge compensation by either ionic or electronic species (eq 11). These results are consistent with experimental studies[3,25] that have already shown compositions with partial or complete substitution of Fe by other divalent cations such as Mn and Co. For example,

(49) Mather, G. C.; Islam, M. S. *Chem. Mater*. **2005**, *17*, 1736.
(50) Wu, J.; Davies, R. A.; Islam, M. S.; Haile, S. M. *Chem. Mater*. **2005**, *17*, 846.
(51) (a) Balducci, G.; Islam, M. S.; Kaspar, J.; Fornasiero, P.; Graziani, M. *Chem. Mater*. **2003**, *15*, 3781. (b) Balducci, G.; Kaspar, J.; Fornasiero, P.; Graziani, M.; Islam, M. S. *J. Phys. Chem. B* **1998**, *102*, 557.
(52) (a) Lewis, G. V.; Catlow, C. R. A. *J. Phys. C: Solid State Phys*. **1985**, *18*, 1149. (b) Tealdi, C.; Islam, M. S.; Malavasi, L.; Flor, G. *J. Solid State Chem*. **2004**, *177*, 4359.

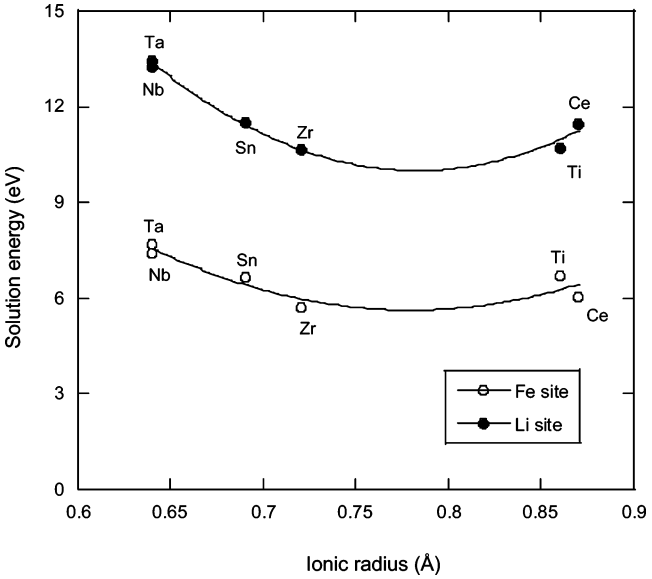


**Figure 6.** Solution energies of tetravalent ions (Sn, Zr, Ti, and Ce using eqs 14 and 15) and pentavalent ions (Nb and Ta using eqs 16 and 17) on Li and Fe sites as a function of ion size. (Lines are a guide for the eye only.)

the Li cycling and electrochemical behavior of the solid solution $LiFe_{1-x}Mn_xPO_4$ ($x = 0$ to 1) have been reported.[3]

Second, high positive values are found for all dopants on Li and for all aliovalent ($M^{3+}$, $M^{4+}$, and $M^{5+}$) cations on Fe (Figures 5 and 6); the lowest energy is found for $Nd^{3+}$ on Fe. It is interesting to note that, although the calculated energies are still high, the smallest dopants (such as Al and Nb) do not show a preference for the Li site, which suggests that ion size is not the dominant factor for the attempted doping of olivine phosphates. The simulations, therefore, indicate unfavorable aliovalent doping (e.g., Al, Zr, Ti, Nb) and suggest insignificant solubility for such dopant species on energetic grounds. These results provide support for studies that suggest that aliovalent dopant substitution in $LiFePO_4$ is unlikely[7−9] and that any enhancement in electronic conductivity may not be a true lattice doping effect.

We note that Chung et al.[6] propose a mechanism whereby cation doping on the M1 sites allows the stabilization of cation-deficient systems such as $Li_{1-a-x}Zr_xFePO_4$ (where $a$ is the Li vacancy concentration); they suggest this is then compensated by mixed-valent $Fe^{2+/3+}$, resulting in p-type conductivity. However, Herle et al.[8] examined the compositions $Li_xZr_{0.01}FePO_4$ ($x = 0.87$ to 0.99) and found that percolating "nano-networks" of metal-rich phosphides within the grain boundaries of $LiFePO_4$ crystallites are responsible for the enhanced electronic conductivity. Recent structural and electrochemical studies of Delacourt et al.[25] were unsuccessful in Nb doping of $LiFePO_4$; instead, they formed crystalline $\beta$-$NbOPO_4$ and/or an amorphous (Nb, Fe, C, O, P) coating around $LiFePO_4$ particles, which is believed to be responsible for the superior conductivity.

In summary, our results suggest that, on energetic grounds, the olivine phosphate $LiFePO_4$ is not tolerant of aliovalent dopant substitution on either Li (M1) or Fe (M2) sites. This is in contrast to the range of dopants that can dissolve into spinel-structured oxides such as $LiMn_2O_4$.

## 4. Conclusions

The present study of the lithium battery material $LiFePO_4$ has used well-established simulation techniques to provide deeper fundamental insight as to the defect, dopant, and lithium ion transport properties on the atomic scale. The following main findings emerge from our investigation:

(1) Our simulation model shows good reproduction of the observed olivine-type structure of $LiFePO_4$. The most favorable intrinsic defect is the Li−Fe "anti-site" pair in which a $Li^+$ (on the M1 site) and an $Fe^{2+}$ (on the M2 site) are interchanged. This type of anti-site defect or "intersite exchange" is well-known in olivine silicates such as $MgFeSiO_4$, although the degree of anti-site disorder is predicted to be much lower in $LiFePO_4$ at ambient temperatures. A relatively low Li Frenkel energy also suggests that a minor concentration of vacancy and interstitial defects could be present.

(2) The lowest $Li^+$ migration energy (0.55 eV) is found for the pathway along the $[010]_{Pnma}$ channel, indicating high lithium mobility, and is consistent with the available measured values. Detailed analysis reveals a nonlinear, curved trajectory between adjacent Li sites. In view of this type of one-dimensional mechanism, anisotropic transport behavior is expected and may be a general intrinsic phenomenon in all isostructural $LiMPO_4$ materials. With such a pathway, however, there is the possibility that long-range $Li^+$ conduction will be easily blocked, for instance, by $Fe_{Li}$ anti-site defects, which would influence the electrochemical kinetics during Li extraction.

(3) A range of dopants with charges varying from +2 to +5 have been examined, constituting a wider survey than current experimental reports. Low favorable energies are found only for divalent dopants on the Fe (M2) site (such as Mg and Mn), which is in accord with experimental work. In general, our results suggest that, on energetic grounds, $LiFePO_4$ is not tolerant to aliovalent doping (e.g., Al, Ga, Zr, Ti, Nb, Ta) on either Li (M1) or Fe (M2) sites; this is compatible with the experimental reports of unsuccessful incorporation of Zr and Nb dopants.

Our study clearly suggests the need for further structural work (e.g., neutron diffraction, Li NMR, EXAFS) to examine defect properties and lithium migration pathways.

**Acknowledgment.** We are grateful to the EPSRC and the Leverhulme Trust for financial support and to L. Nazar and A. Navrotsky for useful discussions.

CM050999V